RADIAL FORCE CHARACTERISTICS OF A SWITCHED RELUCTANCE MACHINE

Neil R. Garrigan Wen L. Soong* Charles M. Stephens Albert Storace** Thomas A. Lipo***

GE Corporate R&D Center
EP Building Room 118
PO Box 8
Schenectady, NY 12301

*Electrical Engineering Dept.
University of Adelaide
Adelaide SA 5005 Australia
(Employed at GE–CRD for this work.)

**GE Aircraft Engines
MD K113
One Neumann Way
Cincinnati, OH 45215

***Dept. of Electrical Engineering
University of Wisconsin–Madison
1415 Engineering Drive
Madsion, WI 53706

***Abstract* – The operation of a switched reluctance machine with eccentric rotor positions creates asymmetrical airgap flux distributions and results in unbalanced magnetic pull. This paper comprehensively investigates the static and dynamic radial force characteristics of an 18/12 switched reluctance machine with unbalanced operation. A powerful magnetic equivalent circuit (MEC) modelling approach is developed and allow fast and accurate force predictions with arbitrary excitation and position. The model calculates the instantaneous radial and tangential forces on the individual poles as well as the net forces on the rotor. The method is validated with finite element analysis (FEA) and against experimental results from a 12/8 machine. Static radial force characteristics are first developed. The MEC is then coupled with a time stepping algorithm to calculate the simultaneously varying electrical, mechanical, and magnetic variables for dynamic operation of the complete SR motor drive. Dynamic radial force behavior is examined, where parallel connected windings are found to naturally and significantly reduce the unbalanced magnetic pull. Variations of radial force with torque−speed operating point are also examined.**

I. INTRODUCTION

Switched Reluctance Machines (SRM's) have been the subject of much active research. Presently they are finding their way into various commercial, industrial, and military applications [1]. Perhaps one of the most established applications is that of a starter/generator for an advanced military aircraft engine. Specific requirements of fault tolerance, high temperature, and high speed make the SR machine a strong candidate for application to aircraft power generation systems [2][3][4]. Additional advantages associated with high speed operation, low friction, and active positioning are realized when the machine is integrated with a magnetic bearing system and located directly on the aircraft engine shaft.

The potential advantages of SR technology present researchers and engineers with some exciting technical challenges in the areas of machine design, controls, power electronic drive circuitry, analysis and system integration to name a few. These areas have been the subject of much research and development. While many of these areas are the subject for ongoing research, little has been done to address the implications of integration with a magnetic bearing system. The magnetic bearing system presents an additional 5 degrees of freedom for the mechanical rotor motion, thus requiring eccentric operation of the SR machine.

The eccentric positioning of the SR rotor creates unbalanced electromechanical radial forces due to asymmetrical magnetic pull. A thorough understanding of unbalanced radial forces and detailed models that can predict them for various modes of operation with various machine geometry is required and could be most useful for studying other conventional SR drive issues, such as the impact of mechanical and manufacturing imperfections on the load and hence life of conventional bearings, and acoustic noise issues.

The principle objective of this research is to characterize the radial force properties of the SR machine associated with eccentric rotor positioning. Radial forces must be predicted and understood for establishing the bearing performance requirements as well as providing a means for compensation of unwanted disturbances to both radial and angular dynamics. To this aim, a versatile magnetic equivalent circuit (MEC) model is developed for the purpose of characterizing the machine behavior under a wide range of operating modes. The model is required to enable fully coupled nonlinear magnetics, arbitrary excitation, and to be capable of predicting the electromagnetic field and electromechanical force production with unbalanced mechanical operation. Additional capability is required to couple with the temporal differential equations of electrical excitation and mechanical motion to provide a fully dynamic simulation tool.

TABLE I
KEY PARAMETERS OF THE 18/12 SWITCHED RELUCTANCE MACHINE

Parameter	Value
Stator outside diameter	33.9cm (13.36")
Rotor outside diameter	25.6cm (10.1")
Stack length	11.4cm (4.5")
Airgap length	0.762mm (0.030")
Maximum expected eccentricity	33% of airgap
Lamination material	Hyperco 50
Rated generating power	250 kW
Maximum operating speed	18,000 rpm
Rated DC bus voltage	270 V
Rated peak pole current	250 A

A series of static force investigations are performed to characterize the radial force properties as a function of instantaneous position and excitation. Particular to this study, is the motivation to examine the dynamic radial force properties for various modes of operation. The results can then be extended to quantify the dynamic stiffness contributed to the entire rotating assembly by the unbalanced SR machine. The models are developed to flexibly cope with various SR machine geometries such as 6/4, 12/8, and 18/12. The results of this effort specifically address an 18/12 250kw machine and provide a comprehensive characterization of the unbalanced radial forces for various mechanical and electrical operating modes. The parameters for the machine under investigation are given in Table I.

0-7803-5589-X/99/$10.00 (c) 1999

II. Magnetic Equivalent Circuit Modelling

A. Circuit Structure

A powerful magnetic equivalent circuit (MEC) based model is developed to provide a versatile means for investigating the unbalanced SR machines of this study. The need for an efficient, accurate and static as well as dynamic model that can cope with the complexity of an entire machine with mechanical or electrical asymmetry motivates the selection of MEC analysis. Magnetic Equivalent circuit modeling affords a good compromise between the accuracy of finite element and the computational speed of analytical models.

The MEC network is designed from the machine geometry and from a "foreknowledge" of the flux paths. The circuit consists of a network of passive permeance elements and active MMF source elements. The passive permeance elements consist of both saturating iron and linear air elements both of fixed and variable geometries. The iron magnetic characteristics are governed by the inherent BH properties of the selected material. The result is a non−linear magnetic circuit including mutual coupling with independent and arbitrary excitation and positioning.

The MEC model can be embedded in a time stepping algorithm for simulation of dynamic behavior coupled at the mechanical and electrical terminals. Fig. 1 illustrates a simplified MEC for a 6/4 SR machine. For convenience of illustration, only core, tooth, and gap flux paths are shown on this diagram. Note that there is individual and independent pole excitation and that there is no symmetry assumed as with most SR models.

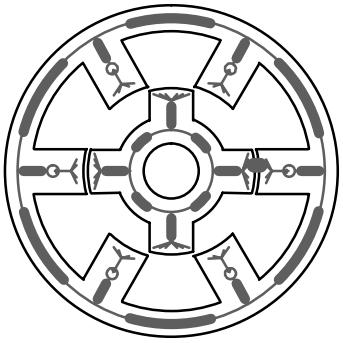

Fig. 1 Simplified MEC representation for a 6/4 SRM

B. Computational Engine

The computational implementation for the model is developed to provide a maximum level of versatility. To this aim, a generic formulation is developed to automatically deal with different machine configurations and operating modes, including geometry, stator/rotor pole number, windings, magnetic material, and excitation. The computational structure is comprised of several key parts based on the structure of Fig. 1.

A detailed definition of the machine parameters and input structure initializes the analysis. Next a set of matrix equations are automatically constructed whose coefficients and inputs are calculated from the instantaneous excitation and position information. A nodal analysis approach is selected for its generality, rigor and ability to handle non−planar circuits, unlike a mesh based circuit approach. A numerical solution algorithm, forming the heart of the computational model, iteratively calculates the instantaneous non−linear magnetostatic solution. A post processing algorithm calculates the desired output variables including individual radial and tangential forces for each pole, net force on the rotor, flux and MMF distributions, flux linkages, etc.. The Maxwell stress tensor combined with an appropriately selected integration path easily enable the force calculations for each pole. Coordinate transformations are utilized to vectorially sum the radial forces to determine the net radial force acting on the rotor body.

III. Finite Element Modelling

An automated 2−D finite−element analysis (FEA) package for switched reluctance machines was prepared by a finite element software company. The package is enormously flexible in evaluating magnetostatic situations. Rotor and stator grids are automatically created from a data file of the machine's major dimensions. The angular coordinate of the rotor and the horizontal & vertical off−center deflections are used to position the rotor grid with respect to the stator grid. The current in each stator coil is individually specified, and this, combined with rotor positioning flexibility, allows a magnetostatic evaluation of any possible situation of an SR machine.

Automatic post−processing calculates the electromagnetic torque and the horizontal & vertical electromagnetic forces from a magnetostatic solution of the machine. The torque and force for each individual rotor pole, as well as a summed total rotor torque and force are calculated. Fig. 2 illustrates the flux plot of an 18/12 SRM with one phase excited for an offset rotor position. Note the greater flux density on the right side of the machine where the airgap is reduced, resulting in an unbalanced magnetic pull.

IV. Flux Linkage Characteristics

The flux linkage characteristics of the SR machine form the heart of virtually all analytical SR models. The flux linkage characteristics indicate much of the principle behaviors of the machine, namely inductance and energy conversion. Unlike the analytical models, the MEC like FEA has the capability to generate the flux linkage curves of the machine. It is therefor fitting, as a first step in verification and calibration of the MEC model, to calibrate the model based on the flux linkage curves of the machine.

The finite element model is used to generate a reference set of curves for comparison. Fig. 3 illustrates the flux linkage characteristics of the machine calculated with rotor position as a parameter for balanced operation. Note that balanced operation here refers to symmetrical electrical excitation of the poles and to a centered mechanical rotor position, i.e. no eccentricity. It is observed that the MEC predictions agree very

0-7803-5589-X/99/$10.00 (c) 1999

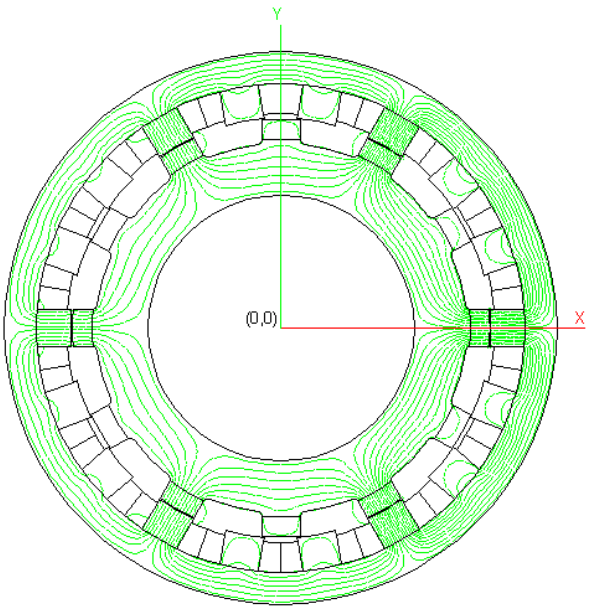

Fig. 2 FEA Flux plot for an 18/12 SRM with a 33% gap eccentricity.

well with those obtained from FEA. This illustrates the capability of the MEC model.

Most SRM modeling techniques require the flux linkage characteristics as an input, whereas the MEC model has inherent capability to predict the characteristics. It should also be noted that in general the flux linkage characteristics are a function of four variables rather than two for the balanced machine. The eccentricity contributes two additional variables to the usual variables of current and angular position. Equation (1) indicates the multi−variable dependency.

$$\lambda = \lambda(i,\theta,x,y) \tag{1}$$

The MEC model must be capable of dealing with the added complexity to accurately model the flux distributions and hence the radial force. In addition to the eccentricity, the poles are able to be independently excited for generality. Typically SR analyses assume symmetrical excitation as well as geometric symmetry and are not capable of dealing with unbalanced and unsymmetrical operation. The capability of the MEC model to deal with these complexities also make it suitable for the investigation of faulted operation, a subject of much interest for the SR machine.

V. Static Radial Force Characteristics

A. Radial Force Computation

Before presenting the predicted radial force characteristics, some explanation of the radial force calculation is in order. The calculation of radial forces are based on the Maxwell Stress Tensor in the developments of this work. Others [5] have presented energy based methods involving the differential variations in the geometric dependent permeance elements, which can be shown equivalent. Since the MEC by nature assumes flux paths apriori to the solution, the assumed

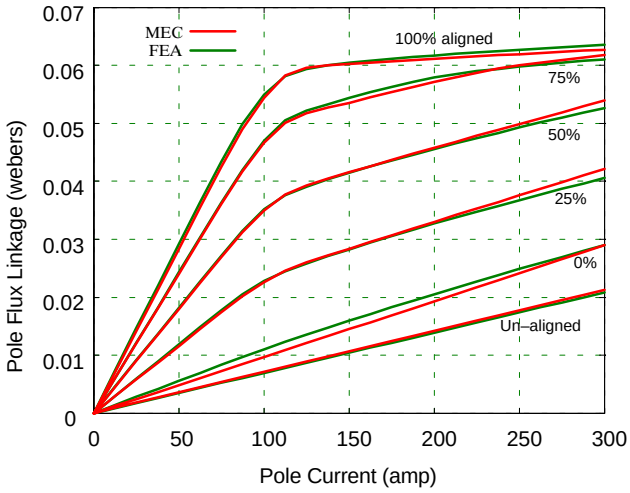

Fig. 3 Flux Linkage Characteristics, 18/12 SRM − Comparison of MEC & FEA

flux lines are well defined and very suitable for application of the Maxwell stress tensor. Together with the appropriate selection of integration paths around the individual pole faces, the Maxwell stress tensor provides straight forward calculation of the radial forces once the magnetostatic solution is obtained. Recall the Maxwell stress tensor as given in (2), where the resultant force is independent of the integration path.

$$F_N = \frac{1}{2\,\mu_o}\int\int_S \left(B_N^2 - B_T^2\right) dA \tag{2}$$

$$F_T = \frac{1}{2\mu_o}\int\int_S B_N\, B_T\; dA \tag{3}$$

To illustrate, consider the alignment of two poles as indicated in the simplistic cartoon representation of Fig. 4. The approximations of the flux paths being always radial across the airgap ease the selection and calculation of the stress contour. The contour is selected such that the flux lines are either orthogonal or parallel to the contour. Under these conditions the Maxwell stress equation simplifies to yield only forces normal to the contour as follows:

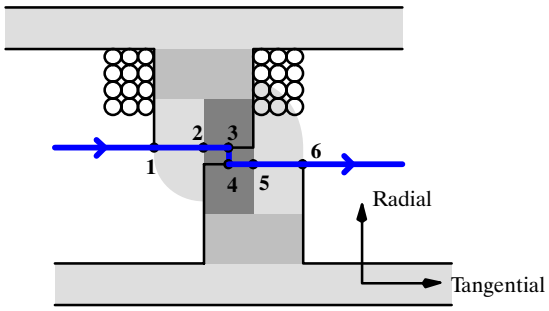

Fig. 4 Application of the Maxwell Stress Tensor in the calculation of radial and tangential forces.

0-7803-5589-X/99/$10.00 (c) 1999

Orthogonal Field Lines: $$F_N = \frac{1}{2\mu_o}\int\int_S B_N^2\, dA \qquad (4)$$

Parallel Field Lines: $$F_N = \frac{1}{2\mu_o}\int\int_S -B_T^2\, dA \qquad (5)$$

Applying these equations to the contour illustrated in Fig. 4 results in the following radial and tangential forces acting on the rotor tooth:

$$F_{radial} = \frac{L_{stack}}{2\mu_o}\cdot\left[\int_1^2 B_{f1}^2\, dl + \int_2^3 B_m^2\, dl + \int_4^5 B_m^2\, dl + \int_5^6 B_{f2}^2\, dl\right]$$

$$= \frac{L_{stack}}{2\mu_o}\left(B_{f1}^2\, l_{12} + B_m^2\,(l_{23} + l_{45}) + B_{f2}^2 l_{56}\right) \qquad (6)$$

$$F_{tangential} = -\frac{L_{stack}}{2\mu_o}\int_3^4 B_m^2\, dl = -\frac{L_{stack}}{2\mu_o}\, B_m^2\, l_{34} \qquad (7)$$

where B_{f1}, B_{f2}, *and* B_m are the first and second airgap fringing fields and the main airgap field, respectively. Thus the radial force is equivalent to integrating $\frac{B_{radial}^2}{2\mu_o}$ over the surface area of the airgap and the tangential force is equivalent to $\frac{\partial W}{\partial\theta}$ where W is the stored energy in the overlapping region of the airgap. Equation (7) and the rotor radius are directly used to calculate the torque as:

$$T = R_{rotor}\, L_{stack}\, B_m^2\, l_{34} \qquad (8)$$

Lastly, all of the force contributions of each active pole pair are combined together to determine the net radial force acting on the rotor body. This entails accounting for the orientation and magnitude of each force. A coordinate transformation local to each pole pair easily maps the local forces to the main x,y stator reference system. The forces and torques are then vector summed. The coordinate transformation for one such pole pair is given as:

$$\begin{bmatrix} Fx_{ref} \\ Fy_{ref} \end{bmatrix} = \begin{bmatrix} \cos\theta i_{jk} & -\sin\theta i_{jk} \\ \sin\theta i_{jk} & \cos\theta i_{jk} \end{bmatrix}\cdot\begin{bmatrix} Fx_{jk} \\ Fy_{jk} \end{bmatrix} \qquad (9)$$

In summary, the application of the Maxwell stress tensor to the well defined magnetic circuit flux paths is appealing, simple and intuitive.

B. *Force –vs– Pole Current*

A fundamental characteristic of the radial forces in the machine as a function of current and eccentricity is the force versus pole current with eccentricity as a parameter. Fig. 5 illustrates the force−vs−pole current for the 18/12 SR machine for two different eccentricities with the machine in the fully aligned position. The plot also compares the predictions of the lumped circuit model with that of finite element. It is observed that the MEC predicts well with the FEA.

Characteristically, the force is observed to rise with the square of current in the linear region as expected, reach a peak and then fall off dramatically with magnetic saturation. The effect of eccentricity is also observed from the plot where an increased rotor displacement produces a larger unbalanced radial force. In the linear region, flux builds linearly with current and hence the force goes as the square. As the knee is reached and the machine begins to saturate, the force peaks. As saturation sets in, the flux tends to equalize around the machine and the unbalance dissipates. In hard saturation, the radial force drops off dramatically. Another view is that in the extreme, the saturation effectively widens the airgap making the eccentricity much effective smaller and the reluctance is balanced around the machine. As expected the largest discrepancies between the two predictions is in the saturated region. Saturation is the most difficult area to accurately match with MEC as the flux paths become much less defined.

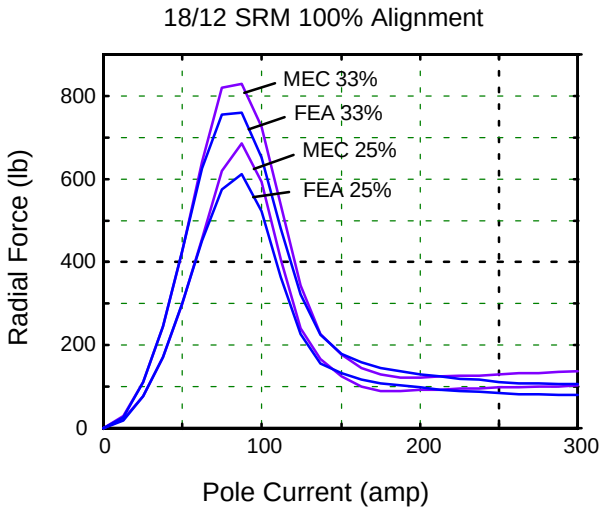

Fig. 5 Radial force −vs− pole current, 18/12 SRM, 25% & 33% gap offset in rotor position.

It is important to recognize that the net radial force is the unbalance of large radial forces on a per pole basis. Fig. 6 illustrates the radial force contributions of the two diametrically opposite poles in line with the eccentricity. The force characteristics of Fig. 5 are more apparent when the individual pole forces are considered.

It should be noted that each point on these curves represents a potential instantaneous point under dynamic operation. Also the peak force here of 800 lbs represents the largest instantaneous force obtained for operation limited to this eccentricity and peak current level. It's also interesting to keep in mind that the worst case radial force does not occur at maximum excitation. These results will be revisited again in the discussion of dynamic operation.

C. *Force –vs– Angular Position*

Another fundamental characteristic is that of the radial force−vs−pole position with eccentricity and current as parameters. Fig. 7 illustrates the radial force for a 33% eccentricity as a function of rotor angular position with current as a pa-

0-7803-5589-X/99/$10.00 (c) 1999

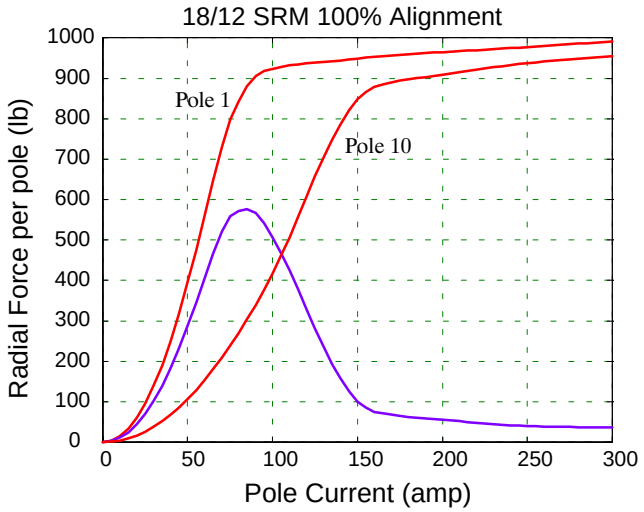

Fig. 6 Radial force per pole –vs– pole current, 18/12 SRM, 25% & 33% gap offset in rotor position.

rameter. In this case one set of poles or one phase is excited with a fixed DC current and then the rotor is rotated from the unaligned position, through alignment and into the next unaligned position. It is observed that the peak forces occur at 100% alignment as expected from Maxwell stress and maximum flux density in the gap.

The dependency on current is also observed in the variation of the radial force levels. The maximum force occurs at the peak force–vs–current levels and 100% alignment as observed on the previous plots. Together this plot and the previous plot indicate that the maximum instantaneous radial force will occur at the aligned position with a pole current of 90 amps. This is to be compared with the rated peak pole current of approximately 250 amps.

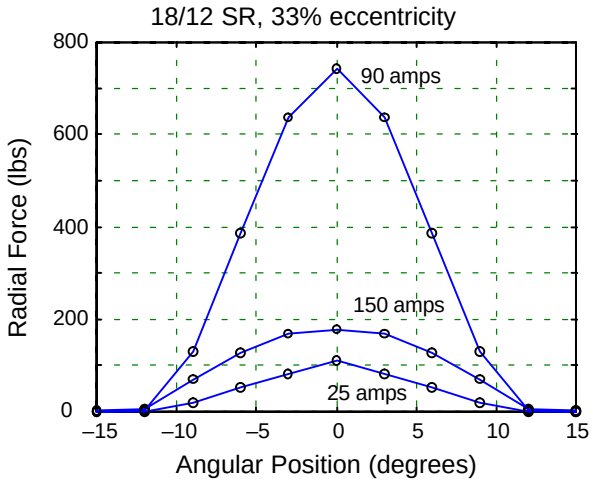

Fig. 7 Radial force–vs–pole position, 18/12 SRM, 33% gap offset in rotor position, FEA results.

D. *Force –vs– Eccentricity*

Lastly to characterize the static radial force properties of the machine is the variation of radial force with eccentricity. In this case the current and the the alignment position are held at the peak producing values, 90 amps and 100% alignment, respectively. Fig. 8 illustrates the results as predicted with the MEC model. As expected, the unbalanced radial force grows almost linearly with increasing eccentricity. At larger displacement the rate of increase in force drops off. This drop off is most likely due to the onset of saturation in the magnetics where the airgap is reduced.

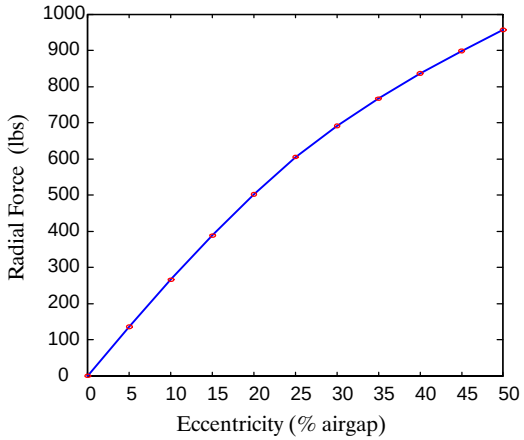

Fig. 8 Radial force–vs–eccentricity, 18/12 SRM, 90 amps and 100% alignment.

VI. Dynamic Radial Force Predictions

A. *Dynamic Modeling*

So far only static characterizations of the SR radial forces have been discussed for specific operating points of position and excitation. It is however of great interest to understand the radial force behavior that occurs as the machine is operated dynamically. This includes commutation, regulation and general operation over the torque–speed operating range.

While the finite element program developed is most accurate for static calculations, it does not perform dynamic analyses. In order to perform dynamic time domain simulations, a time stepping finite element program would be required. Although the results would be very accurate, the already long static computation time would become unacceptable for the present computing capabilities available, especially for the numerous and varied cases considered for an integrated magnetic–bearing/starter–generator system.

The lumped magnetic equivalent circuit model (MEC model) is much faster than FEA with minimal compromise in accuracy and can be coupled to the temporal electrical and mechanical differential equations. This enables time domain simulation with unbalanced mechanical and/or electrical conditions and dynamic prediction of radial forces. To this end, algebraic equations of the static model are coupled to the temporal differential equations of the electrical and mechanical terminal variables and embedded into a time–stepping algorithm to form a complete dynamic system simulation.

Fig. 9 illustrates the MEC model embedded into a dynamic simulation model including the SR commutation and torque

0-7803-5589-X/99/$10.00 (c) 1999

control algorithms, and the mechanical dynamics. This forms the most powerful aspect of the MEC model, its ability to combine computational speed with modelling accuracy and predict the simultaneously varying dynamic behavior of the electrical, mechanical, and magnetic variables coupled to the entire switched reluctance drive system. To the authors' knowledge, no other model of this capability has been developed for the SR machine.

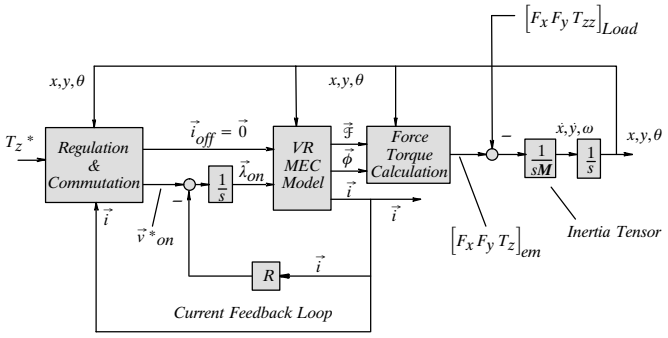

Fig. 9 Dynamic simulation model of the SR system.

B. Current Source Excitation

The first dynamic case to be considered is that of current source excitation. In this case ideal current source excitation is assumed and the poles of each phase are forced to have equal currents. Since the magnetic circuits will not be symmetrical due to the eccentricity, a flux distortion and hence unbalanced radial forces are expected around the circumference of the machine. Current excitation is approximated at low speed operation of the machine where the current regulation is very strong. In the case where the poles of each phase are connected in series, the currents are forced to be the same in each pole. Current source excitation is a worst case scenario as in general voltage constraints require the poles to be connected in some parallel fashion which exhibits inherent flux balancing.

To further validate the force calculations, the current waveforms are analyzed statically on a point−by−point basis with the FEA model. A current waveform as a function of position or time obtained from a simulation or from real data is forced into each winding equally for a point−by−point calculation with FEA. This gives somewhat of a quasi−dynamic FEA solution. Fig. 10 illustrates the forces as calculated with FEA and the MEC model. This is the first calculation of this paper shown to account for the forces contributed spatially for all of the poles and phases as they are sequentially excited. The plot illustrates very good agreement between the FEA and MEC predictions. Observe that the force pulsates at a rate equal to the number of rotor poles times the number of phases times the synchronous speed (3x12xRPM = 7.8kHz in this case, and 10.8kHz at the maximum speed of 18kRPM). The radial force is also observed to have an average or DC value. The force is virtually all in the direction of the eccentricity. As shown the y−directed force is very low in amplitude with virtually no DC value. The average radial force in the x−direction is 303 lbs for the FEA data and 307 lbs for the MEC data. It should be noted that each instantaneous point on the plot in Fig. 10 corresponds to a condition represented in the series of static characteristics previously presented.

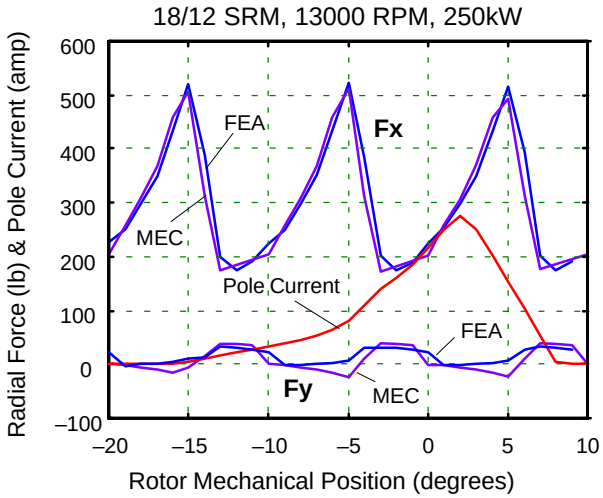

Fig. 10 Radial force with dynamic current source excitation, 18/12 SR machine with 33% gap offset.

C. Voltage Source Excitation

A more realistic case to be investigated is that of voltage mode excitation with parallel connected poles. This is the true physical means by which the machine will be excited. Even with current regulators, the applied forcing function to the machine terminals is still voltage. This dynamic analysis can only be performed with the MEC model. To illustrate the influence of parallel windings and the capability of the MEC model, the same simulation is repeated for voltage mode excitation. With voltage excitation, the voltage and hence approximately the fluxes are equal and the currents distribute according to inductance or relative airgap. This is a self compensating affect that tends to reduce the radial forces under certain modes of operation. Now the currents are allowed to automatically adjust themselves according to the relative airgaps around the machine.

The same firing angles from the current excitation case were used for voltage excitation. The radial force is plotted in the Fig. 11 and is observed to be reduced from that of the current mode case. An average radial force of 88 lbs is obtained from the MEC dynamic analysis. It should be noted that even if the external terminals were excited with a current source, the currents would still divide asymmetrically according to the unbalance in inductances if the poles are connected in parallel. An natural flux balancing would still occur and the radial forces would be reduced from the series connected case. Generally speaking, poles are connected in parallel rather than series to conform to the voltage and current constraints of the power electronics that typically favor lower voltage.

0-7803-5589-X/99/$10.00 (c) 1999

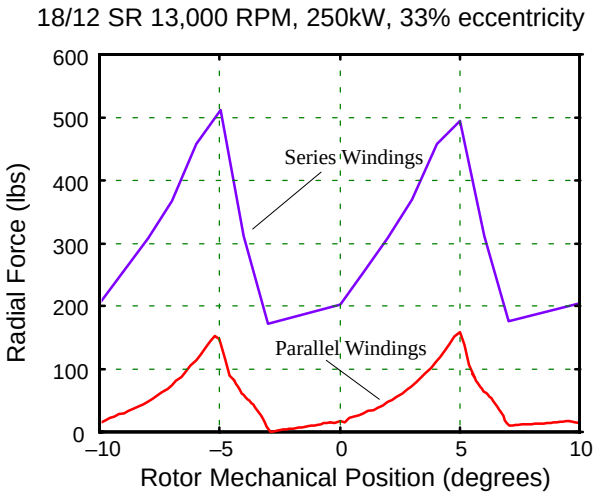

Fig. 11 Dynamic radial force comparison for voltage and current source excitation.

VII. Radial Force Frequency Response

A. Motivation

So far the dynamic analyses indicate that the radial force appears as a negative stiffness in the direction of the eccentricity. However, the eccentricity has only been treated statically. That is the rotor has been offset from its centered position and then spun about its geometric center. When integrated with a magnetic bearing system, the eccentricity will also be a dynamic variable. In the case of a whirl condition, the eccentricity will be a rotating vector. The whirl may be forwards, backwards, synchronous, sub−synchronous or super synchronous. The whirl can also be a harmonic combination of various frequencies. The realistic expectation of these scenarios raises the question of the frequency response for the radial force.

While the radial force can essentially be mapped as a negative stiffness varying with the torque−speed operating point, the frequency response of the force will be of primary interest from the rotordynamics point of view. The influence of whirl and stability will be the key motivations regarding rotordynamics analyses. Considering a whirl condition, the eccentricity of the rotor is changing with time. In any one radial direction the eccentricity will be a harmonic sinusoidal function in time. Thus it is important to consider the response of the radial force to perturbations in the eccentricity. The capability of such an analysis again indicates the versatility and power of the MEC model coupled to a time stepping electrical and mechanical simulation.

B. Simple Analytic Model

Without proceeding to the full MEC model, a good indication of the response can be derived from some simple physical equations and some basic assumptions. Since the force is dependent upon flux established in the magnetic circuit, the frequency response of the radial force is expected to essentially be an RL response. A circular whirl will appear as two orthogonal (sin & cosine) functions in the x & y radial directions. Considering one eccentricity direction only, neglecting the leakage flux and eddy currents, and assuming radial flux in the overlap region only, a few physical equations can quickly reveal the form of the radial force frequency response. These equations are derived as follows for a single magnetic path in the electrical machine:

$$v = iR + \frac{d\lambda}{dt} \tag{10}$$

$$\lambda = \lambda(i,x,y,\theta) \quad \text{and} \quad i = i(\lambda,x,y,\theta) \tag{11}$$

$$F = \frac{B^2}{2\mu_o}A = \frac{\lambda^2}{2\mu_o N^2 A} \tag{12}$$

Note that the flux linkage is, in general, a function of four variables. The following analysis will only consider perturbations in flux and one radial direction, hence the other two variables will be dropped from the notation.

Linearization of the preceding equations results in the following small signal equations that govern the behavior for small excursions about an operating point.

$$\Delta v = \partial\frac{i(\lambda,x)}{\partial\lambda}\Delta\lambda R + \partial\frac{i(\lambda,x)}{\partial x}\Delta x R + \frac{d\Delta\lambda}{dt} \tag{13}$$

$$\Delta F = \frac{\lambda_o}{\mu_o N^2 A}\Delta\lambda \tag{14}$$

Finally, the transfer function from the position to the radial force is derived as follows:

$$\frac{\Delta F}{\Delta x}(s) = -\frac{\lambda_o}{N^2\mu_o A}\left[\frac{R\frac{\partial i(\lambda,x)}{\partial x}}{s + R\frac{\partial i(\lambda,x)}{\partial\lambda}}\right] \tag{15}$$

It is evident from (15) that the radial force frequency response is essentially the same as that of the flux linkage or current of an RL circuit, where $\frac{\partial i(\lambda,x)}{\partial\lambda}$ is the incremental inductance reciprocal.

While this result is quite simple, it should be kept in mind that it represents a linearized solution about an operating point for just two pole pairs. Considering the entire machine, there will be a much more complex magnetic circuit active including multiple pairs of excited poles. Additionally, a whirl condition may have a considerably sized amplitude that exceeds the small signal approximation of this analysis. A detailed simulation of the machine in such a condition is required to rigorously address the frequency response properties for eccentricity variations. While the preceding analytical model is far less complex, reasonable results are obtained from this simple representation. Additionally, the extremes of the response can be quite accurately assessed as given in the next section.

C. Frequency Response Predictions

A simulation model based on the machine parameters, flux linkage characteristics, and the analysis of the preceding section is used to investigate the frequency response of the radial force. Specifically a perturbation is given in the eccentricity

0-7803-5589-X/99/$10.00 (c) 1999

and the radial force is taken as the output. Several operating points on the flux linkage curve are investigated to reveal the rough envelope of response characteristics. Note that no current regulation is assumed, this is only the physics of the machine.

Fig. 12 illustrates the simulation results for various operating points ranging from maximum to minimum incremental inductance. The magnitude and phase of the complex dynamic stiffness are plotted in typical Bode format. Additionally as common to rotordynamic analyses, the real and imaginary parts are plotted as stiffness and damping. Note that the imaginary part is scaled by frequency to give equivalent damping. It should be observed that the inherently high inductance and low resistance of the machine result in substantially low break frequencies. Addition of the current regulator will increase the break frequencies substantially. Even so, the results indicate that the SR radial forces do not act purely as a negative stiffness in the direction of the rotor offset for the case of dynamic eccentricity, such as whirl.

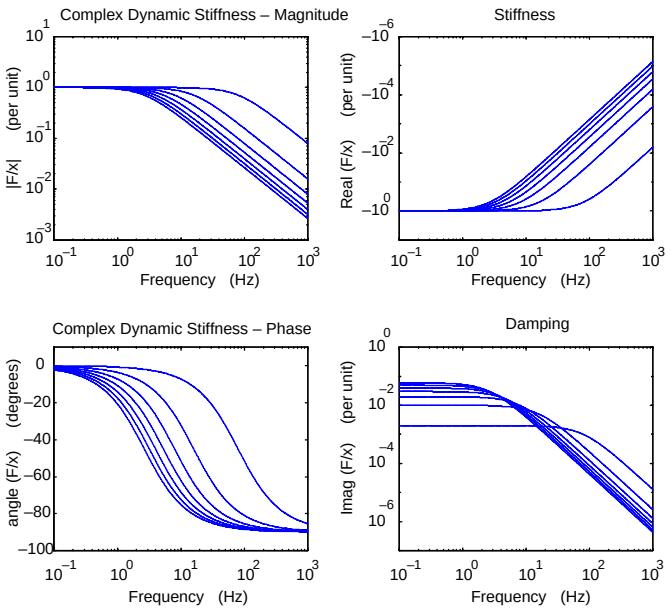

Fig. 12 Radial force frequency response to eccentricity variations.

D. Rotordynamic Implications

The unbalanced radial force is of certain importance to the rotordynamic consideration of the mechanical rotor system. The radial force presents additional loading to the magnetic bearings that must be sized to account for the force if not compensated. Additionally, the radial force is a negative stiffness which is a destabilizing property. The pulsating nature of the radial force as the machine is operated dynamically, presents the potential for excitation of various resonant modes. Since the frequency is synchronous to the spin speed and 36 times higher, it varies continuously and will inevitably pass through a wide range of frequencies and critical speeds of the rotor.

The frequency response as discussed in the previous section implies a phase shift in the radial force under dynamic eccentricity conditions, namely whirl. The phase shift in turn implies an effective damping. This damping has the potential to be positive (stabilizing) or negative (destabilizing). The RL nature of the time constant suggests that the response will be typically very fast as compared to the time constants of the mechanical system. Even so, the complexities associated with the highly non−linear behavior of the magnetics, machine operating modes (i.e. commutation, etc.), and complex rotordynamic interactions maintain significant challenge in understanding the behavior of the system and potentially in the satisfactory operation of the system.

VIII. Radial Force and the Torque–Speed Operating Range

It is of interest to map out the radial force as a function of torque−speed operating point for the starter/generator. Fig. 13 illustrates a surface plot of the predicted unbalanced radial forces as a function of the torque−speed operating point. As expected, the radial force falls off dramatically with increasing speed due to voltage mode excitation. At lower motoring speeds, the current regulators are effective and create larger flux imbalances and hence higher unbalanced radial forces. In particular, the unbalanced radial force is largest at low speeds and reduced torques. This characteristic corresponds to the peaking observed in Fig. 5 at the onset of saturation. The radial force envelop is also observed to change as the motor corner speed is approached. This change is due to saturation of the current regulators giving rise to partial voltage model excitation.

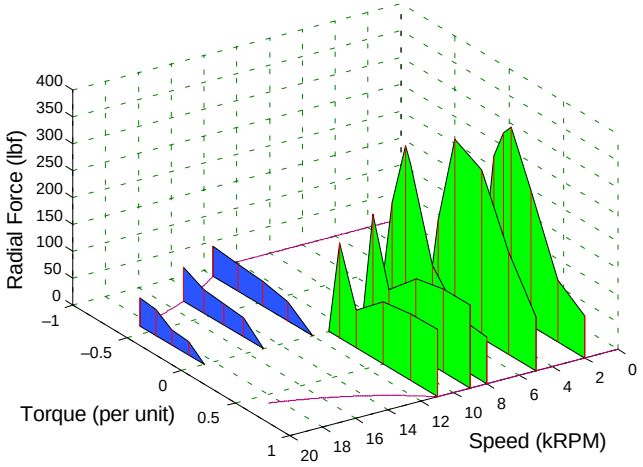

Fig. 13 Radial force −vs− Torque−speed operating point, 18/12 SRM, 33% eccentricity.

IX. Experimental Radial Force Measurements

To gain further confidence in and validation for the radial force predictions, a commercially available 12/8 test motor was experimentally investigated. The motor is considerably smaller than the 18/12 machine and is fabricated from more conventional materials. Simple pull−force tests were performed on the test motor to generate the force−vs−current characteristic plots as predicted for the 18/12 machine in Fig. 5. A finite

0-7803-5589-X/99/$10.00 (c) 1999

element model of the test machine was developed based on measured dimensions and with an assumed magnetic material. Fig. 14 illustrates the experimental and analytical results. The results confirm the qualitative nature of the force−vs−current characteristic. The discrepancy in absolute accuracy is most likely due to the measurement procedure and to inexact BH data. While additional experimental results are not available at this time, the finite element results have been useful in the verification of the MEC model.

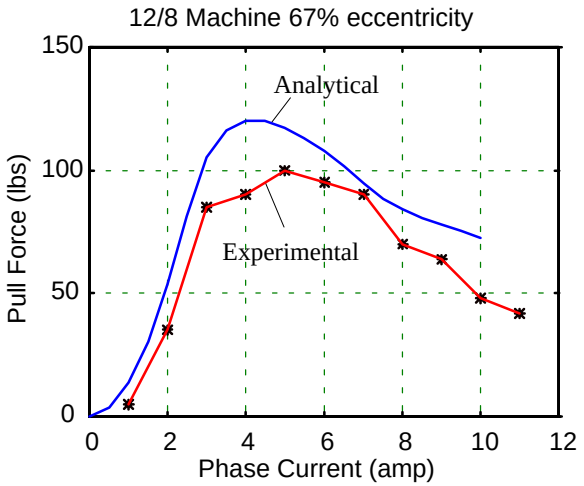

Fig. 14 Predicted and measured radial force −vs− current for a 12/8 SR test machine.

X. Conclusions

A powerful magnetic equivalent circuit model has been described and employed to investigate the static and dynamic unbalanced magnetic radial force properties of a 250kW integral starter generator switched−reluctance machine operating with asymmetrical mechanical rotor positions.

The static unbalanced radial forces as a function of excitation, rotor angular position, and eccentricity has been predicted and validated with finite element results. The magnetic model was then integrated with temporal differential equations to produce a complete time stepping simulation of the SR drive system with the capability of modelling asymmetrical rotor operation.

The dependency of radial forces on the torque−speed operating point as well as excitation mode and winding configuration has been investigated. Specifically, it has been determined that voltage mode excitation of the machine with parallel connected windings has inherent flux balancing and results in substantially reduced radial forces (by a factor of three or four) from that of series connected windings. Finally, limited experimental results with a 12/8 test machine confirm the static analytical predictions.

The model shows that the expected level of radial forces is such that it will be beneficial to utilize some means of radial force compensation in a magnetic bearing switched−reluctance system. Future work will utilize the model to investigate the performance of alternative compensation techniques.

Acknowledgements

A majority of this work was carried out under funding provided by a Navy program awarded to GE Aircraft Engines by the Naval Air Warfare Center−Aircraft Division, Patuxent River, Md., 20670−5304. The contributions, suggestions, and encouragement of Ms. Pauline Tarantini and Mr. Darrell H. Grant, the Navy Program Managers, are greatly appreciated. In addition, the authors would like to thank Scott Rubertus, Jack Geis, Nelson Forster, and Jon Dell of the Airforce at WPAFB, Dayton, Ohio for their support and motivation in understanding the nature of aircraft engine switched reluctance starter/generator machines.

Special recognition is extended to Dr. Eike Richter for the detailed electromagnetic design of the SR machine. Acknowledgements are also extended to Sky Blue Systems for preparing the finite element program. The insights of Dr. Art Radun and Dr. Iqbal Husain are appreciated. Mr. Kevin Gavel and Mr. Marlin Stanly are appreciated for their performance in the experimental testing of the 12/8 machine.

References

[1] T.J.E. Miller, Textbook: *"Switched Reluctance Motors and their Control"*, Oxford University Press, 1993.

[2] E. Richter, "Switched Reluctance Machines for High Performance Operations in a Harsh Environment − A Review Paper", Invited Paper at the International Conference on Electrical Machines (ICEM 90), Boston, MA, 1990

[3] A.V. Radun, "High−Power Density Switched Reluctance Motor Drive for Aerospace Applications", *IEEE Transactions on Industrial Applications, VOL. 28, No. 1,* January/February 1992

[4] J.A. Weimer, *"Electrical Power Technology for the More Electric Aircraft"*, AIAA, 12th Digital Avionics Systems Conference, 1993.

[5] V. Ostovic, Textbook: "Dynamics of Saturated Electric Machines", Springer−Verlag, 1989

[6] J.C. Moreira and T.A. Lipo, " Simulation of a Four Phase Switched Reluctance Motor Including the Effects of Mutual Coupling", *Electric Machines and Power Systems,* Hemisphere, 1989, 16:281−299.

[7] M.A. Preston, J.P. Lyons, "A Switched Reluctance Motor Model with Mutual Coupling and Multi−Phase Excitation", *IEEE Transactions on Magnetics, Vol. 27, No. 6, November 1991.*

[8] T.A. Lipo, *ECE 713 Class Notes − 1995,* Chapter 9, University of Wisconsin − Madison.

[9] T.E. Stern, Textbook: *Theory of Nonlinear Networks and Systems − An Introduction*, Addison−Wesley, 1965

[10] C.J. Carpenter, "Surface Integral Methods of Calculating Forces on Magnetized Iron Parts", *The Institute of Electrical Engineers, Monograph No. 342, August 1959*.

[11] P. Hammond, "Mechanical Forces in Magnetic and Electric Devices", *Electrical Review, Nov. 1961, pp. 733−737.*

[12] K.Takayama, Y. Takasaki, R. Ueda, T. Sonoda, "Thrust Force Distribution on the Surface of Stator and Rotor Poles of Switched Reluctance motor", *IEEE Transactions on Magnetics, Vol.25, No.5, September 1989.*

[13] T.J.E. Miller, "Faults and Unbalanced Forces in the Switched Reluctance Machine", *IEEE Transactions on Industry Applications, Vol. 31, No. 2, March/April 1995.*

[14] Akira Chiba, M. Hanazawa, T. Fukao, M.A. Rahman, "Effects of Magnetic Saturation on Radial Force of Bearingless Synchronous Reluctance Motors", *IEEE Transactions on Industry Applications, Vol. 32, No.2, March/April 1996.*

0-7803-5589-X/99/$10.00 (c) 1999